Highlights on Spanish Astrophysics X, Proceedings of the XIII Scientific Meeting of the Spanish Astronomical Society held on July 16 – 20, 2018, in Salamanca, Spain. B. Montesinos, A. Asensio Ramos, F. Buitrago, R. Schödel, E. Villaver, S. Pérez-Hoyos, I. Ordóñez-Etxeberria (eds.), 2019

Lightening up Dark Galaxy candidates beyond redshift 3 with MUSE.

Raffaella Anna Marino[1], Sebastiano Cantalupo[1], Simon Lilly[1] and the MUSE collaboration.

[1]Department of Physics, ETH Zürich,Wolfgang−Pauli−Strasse 27, 8093 Zürich, Switzerland

Abstract

Theoretical models suggest that each galaxy pass through a 'dark galaxy' phase of formation that involves an epoch when galaxies are gas-rich but inefficient at forming stars. Here, I present the new results published in Marino et al. 2018 on the search for dark galaxies at high redshift ($z > 3$) from the analysis of six MUSE (Multi Unit Spectroscopic Explorer) deep fields. In particular, we take advantage of the quasar-induced fluorescent Lyman α emission to detect and study these otherwise invisible objects to our optical telescopes. In addition, contrary to previous studies based on deep narrow-band (NB) imaging, our integral field survey has several advantages including a nearly uniform sensitivity coverage over a large volume in redshift space as well as full spectral information at each location. Specifically, in Marino et al. 2018, we study the rest-frame equivalent width (EW_0) distributions of the Lyα sources detected in proximity to the quasars and in control samples. We find a clear correlation between the locations of high EW_0 objects and the quasars. This correlation is not seen in other properties such as Lyα luminosities or volume overdensities, suggesting their possible fluorescent nature. Our main result is the discovery of 8 Lyα sources without continuum counterparts and EW_0 limits larger than 240 Å that, so far, are the best and only candidates for dark galaxies at $z > 3$.

1 Introduction

A substantial effort, both observationally and theoretically, has been done in the past decade with the aim to characterize the fuel for the formation of the first stars, i.e. the cold gas ($T \sim 10^4$ K) surrounding the galaxies. However, due to small sample sizes and technical limitations of the current facilities [9], our knowledge about the nature of the Intergalactic Medium (IGM) and Circumgalactic Medium (CGM) at high redshift ($z > 3$) is still limited.

Theoretical models have suggested the existence of a primordial phase (which is almost optically dark) in galaxy formation where gas-rich galaxies reside in low-mass halos (e. g.,

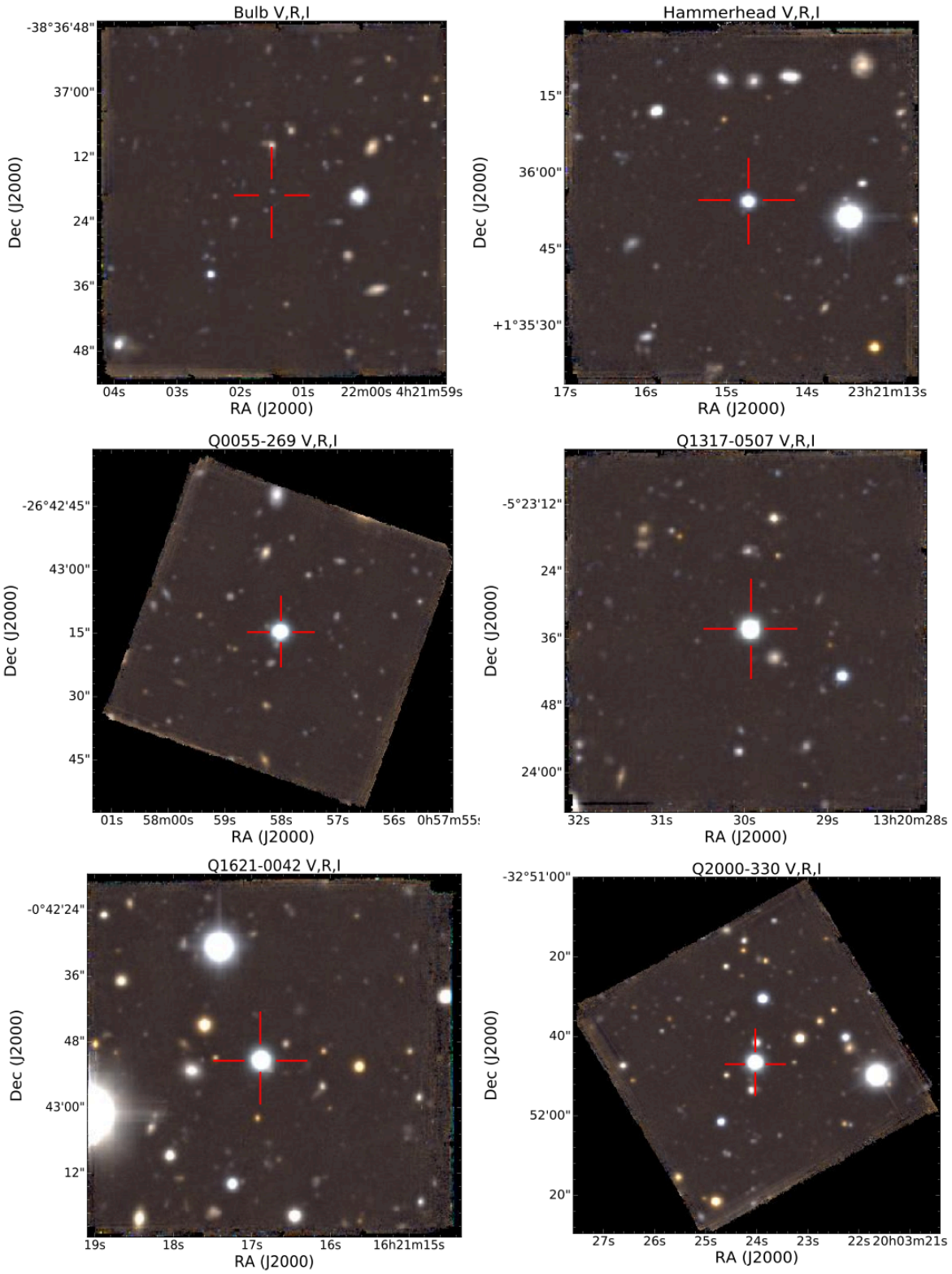

Figure 1: Composite pseudo−color images of the MUSE fields. The RGB colors correspond to the V-, R-, and I-band images obtained from the MUSE datacubes. Each image is 60" ×60" and the red cross indicates the AGN/QSO location. North is up and East is left.

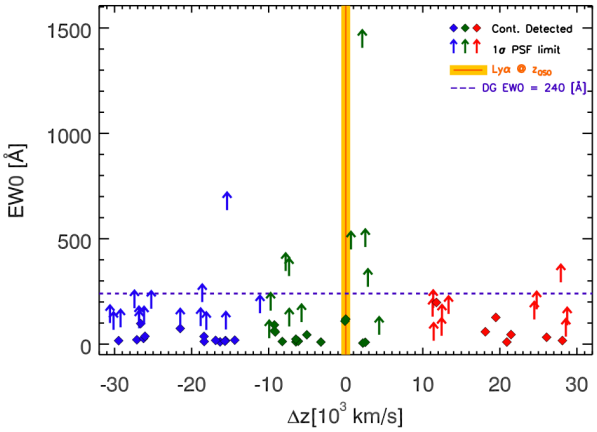

Figure 2: MUSE high$-z$ EW$_0$(Lyα) distribution versus the spectral distance (velocity) from the QSO. Blue and red symbols represent those LAEs detected in the control samples, while green symbols indicate the LAEs closer to the QSO. Diamonds symbolize those LAEs with continuum counterparts, and with the arrows the lower limit (at 1σ) EW$_0$ values for continuum undetected LAEs are plotted. The QSO velocity position (plus the 1σ error) is shown with the shaded yellow area. The horizontal dashed line denotes the EW$_0$ threshold (240 Å) for the Dark Galaxy candidates.

[8, 12, 13]) with very low star formation efficiencies (SFEs=SFR/M$_{\rm gas} < 10^{-11}$ yr^{-1}). This less efficient star formation phase of the IGM gas at high redshift could depend on several factors, including the metal-free gas present in the environment at that epoch, the H_2 self-regulation effect or the reduced CGM cooling rate [5].

Different approaches have been taken to further investigate this dark phase of galaxy formation in the literature, but in most of the studies conducted so far, the proto-galactic phase preceding the first spark of star formation (SF) has been poorly constrained. The different methods that have been used in the past to try to detect the "starless" IGM gas, are summarized in [15]. In our case, we make use of the QSO-induced fluorescent Lyα emission that can locally boost the signal from dense and otherwise optically-dark gas clouds by orders of magnitude [10, 3, 6, 11, 16] acting as a flashlight on its surroundings. Moreover, we use an alternative approach to narrow band imaging to search for the fluorescent Lyα emission, by using the MUSE instrument [1]. MUSE has several advantages over previous instrumental techniques: (1) homogeneous data quality, (2) large wavelength range (which means a large cosmological volume) and (3) provides 2D information for robust analysis, enabling us to investigate how the IGM gas is converted into stars. More importantly, the use of Integral Field Spectroscopy (IFS) provides the ability to build control samples under the same instrumental and observational conditions, as well as data reduction and analysis techniques, with respect to the main dataset.

2 Data and Analisis

In Marino et al. 2018, we study six QSO medium-deep ($\sim$10 hr each) fields at $z > 3$ part of MUSE Guaranteed Time Observation (GTO) program. The observations comprise 270

exposures ($\approx$ 65 hours) in total. Each MUSE datacube is made of 321×328 spaxels with a sampling grid of $0.2" \times 0.2" \times 1.25$ Å yielding $\sim$90,000 spectra per frame. The composite pseudo-color images computed from the MUSE datacube combining the broad V-, R- and I-band images are shown in Figure 1.

The reduction of all 65 hrs of the MUSE data was performed using both the latest version of the ESO MUSE Data Reduction Software (DRS, pipeline version 1.6, [18]), complemented with the `CubExtractor` package (`CubEx` hereafter; Cantalupo, in prep.). We use the DRS routine *MUSE scibasic* for the master-bias, the master-flat, the twilight and illumination corrections, and wavelength calibration. The individual datacubes are created with the *MUSE scipost* routine after performing the flux calibration, together with the geometry and astrometry corrections. Next, we performed the post-processing using several routines of the `CubEx` package in order to improve the automatic flat-fielding correction, the pipeline sky subtraction and to combine the different exposures into the final datacubes (see [15] for further details). The analysis of the six fields comprises the Point Spread Function (PSF) subtraction, to ensure minimum contamination from the QSO PSF in our LAEs detection as well as the subtraction of the brightest foreground continuum sources, again using the `CubEx` tools. Subsequentaly, we build three different sub-cubes from each datacube with the same spectral width 200 Å (or 160 spectral pixels). The on-source datacube is centered on the QSO Lyα wavelength. Two control sample adjacent to the on-source datacube were extracted on the blue and red sides. We blindly implemented 3D source detection on the 18 reduced and post-processed datacubes using `CubEx` with the same threshold parameters ((I) a minimum of 40 connected voxels above a (II) signal-to-noise ratio (SNR) threshold of 3.5 and (III) a SNR measured on the Lyα emission line from the 1D extracted spectrum above 4.5). Finally, we obtained a full catalog of $\sim$ 200 line emitters automatically detected in the on-source and control sample datacubes over the six MUSE fields. Specifically, in a total volume of $\sim$90 physical Mpc^3, we found 186 LAEs, 25 [O II], 13 [O III] emitters and 8 AGN candidates.

3 Lyα equivalent width distribution

Here we only present the equivalent width (EW) results because of space limitation and the reader is referred to the original paper for a complete overview of the dark galaxies results [15]. In order to compute the rest-frame equivalent width, EW$_0$(Lyα), of our targets, we decide to follow two different approaches depending on the detection (or not) of our LAE in the continuum image. A LAE is defined as continuum detected (CD) if its continuum flux measured within the PSF size aperture is higher than 3 times the standard deviation, i.e. the local noise *std*, of the continuum image otherwise the LAE is considered continuum undetected (CU). Of the 186 LAEs selected in our sample, 54% were undetected in the continuum. In the case of the continuum detected LAEs, we used the matched-aperture approach as in [6] while for those LAEs undetected in the continuum image, we used the PSF$-$aperture approach (see [15] for a detailed description of the EW$_0$(Lyα) measurements).

In Figure 2, we present the measured EW$_0$(Lyα) values and limits as a function of the distance (velocity) from the QSO of the high redshift sample (i. e. Q1317, Q0055, Q1621, Q2000 fields at $z > 3.2$). The vertical yellow shaded area marks the position of the QSO.

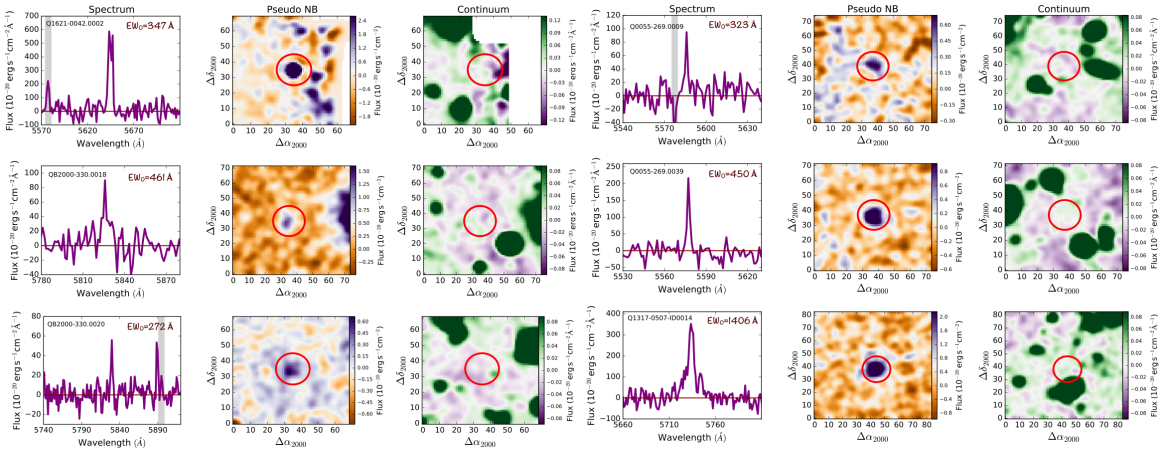

Figure 3: Dark Galaxy candidates detected in the MUSE high−z fields. For each DG, a zoom in of the MUSE spectrum around the observed Lyα emission wavelength, the MUSE Lyα pseudo narrow−band images and the continuum broad−band image obtained from the MUSE datacube are shown. The position of the candidate is marked by the red circle. In each panel North is up and East is left. Plate scale is 0.2"/pix.

The CD LAEs are shown with diamond symbols while the arrows represent the lower limit EW_0(Lyα) estimations for the CU LAEs. Green colors indicate the LAEs detected in the on-source (QSO) samples, while the blue and the red ones represent the control samples. The horizontal dashed line at 240 Å denotes the EW_0(Lyα) limit expected for galaxies with PopII stellar population ([7, 14]). In all MUSE high−z fields we clearly see a higher occurrence of objects with EW_0(Lyα)$>$ 240Å closer to the QSOs rather than in the control samples.

In particular, for the MUSE high−z fields we found that 8 LAEs present a lower limit on their EW_0(Lyα) larger than 240 Å, and 6 of them are observed in proximity of the quasars. In Figure 3, we show the spectra and postage stamps of these 6 high EW_0 objects, a.k.a Dark Galaxies, detected in the high redshift samples.

4 Conclusions

Making use of medium-deep ($\sim$10 hr) MUSE GTO observations around five bright QSOs and one Type-II AGN, we have searched for fluorescently illuminated Dark Galaxies at $z >$ 3.2 among Lyα emitters in proximity of the quasars. Within a volume of 90 physical Mpc^3, we have detected $\sim$ 200 line emitters. We estimated their EW_0(Lyα) in a homogenous way among the main and the control samples using two different approaches depending on the detection in the continuum of each source. In particular, we found 11 objects with EW_0(Lyα) lower limits larger than 240 Å. The analysis of the EW_0(Lyα) distribution revealed that these high EW_0 LAEs tend to preferentially reside within $\sim 10^4$ km/s from the quasar systemic redshift. This excess of high EW_0 sources correlated with distance from the quasar

is completely consistent with the expectations of quasar fluorescent illumination (e.g., [2, 6, 4, 17]). Therefore, the 8 LAEs with $EW_0(Ly\alpha) > 240$ Å and without the continuum counterpart located in close proximity of the QSOs represent the best and only candidates up to date for Dark Galaxies at $z > 3$ (see Marino et al. 2018 for more details).

Acknowledgments

This work is based on observations taken at ESO/VLT in Paranal and we would like to thank the ESO staff for their assistance and support during the MUSE GTO campaigns.

References

[1] Bacon, R., Accardo, M., Adjali, L., et al. 2010, Proc. SPIE, Vol. 7735, 773508

[2] Borisova, E., Lilly, S. J., Cantalupo, S., et al. 2016b, ApJ, 830, 120

[3] Cantalupo, S., Porciani, C., Lilly, S. J., & Miniati, F. 2005, ApJ, 628, 61

[4] Cantalupo, S., Lilly, S. J., & Porciani, C. 2007, ApJ, 657, 135

[5] Cantalupo, S. 2010, MNRAS, 403, L16

[6] Cantalupo S., Lilly S. J., Haehnelt M. G., 2012, MNRAS, 425, 1992

[7] Charlot, S., & Fall, S. M. 1993, ApJ, 415, 580

[8] Dekel, A., Birnboim, Y., Engel, G., et al. 2009, Nature, 457,451

[9] Fumagalli, M., Hennawi, J. F., Prochaska, J. X., et al. 2014, ApJ, 780, 74

[10] Haiman, Z., & Rees, M. J. 2001, ApJ, 556, 87

[11] Kollmeier, J. A., Zheng, Z., Davé, R., et al. 2010, ApJ, 708, 1048

[12] Krumholz, M. R., & Dekel, A. 2012, ApJ, 753, 16

[13] Kuhlen, M., Madau, P., & Krumholz, M. R. 2012, ApJ, 776, 34

[14] Malhotra, S., & Rhoads, J. E. 2002, ApJL, 565, L71

[15] Marino, R. A., Cantalupo, S., Lilly, S. J., et al. 2018, ApJ, 859, 53

[16] Martin, N. F., Ibata, R. A., Rich, R. M., et al. 2014, ApJ, 786, 106

[17] Trainor, R. F., & Steidel, C. C. 2012, ApJ, 752, 39

[18] Weilbacher, P. M. 2015, Science Operations 2015: Science Data Management, Zenodo, doi:10.5281/zenodo.3465